

# Modification of Axial Fan Flow by Trailing Edge Self-Induced Blowing

**Matjaž Eberlinc**

e-mail: matjaz.eberlinc@fs.uni-lj.si

**Brane Širok**

e-mail: brane.sirok@fs.uni-lj.si

**Matevž Dular**

e-mail: matevz.dular@fs.uni-lj.si

**Marko Hočevar**

e-mail: marko.hocevar@fs.uni-lj.si

Faculty of Mechanical Engineering,  
University of Ljubljana,  
Aškerčeva 6,  
Ljubljana SI-1000, Slovenia

*Axial fans often show adverse flow conditions at the fan hub and at the tip of the blade. The modification of conventional axial fan blade is presented. Hollow blade was manufactured from the hub to the tip. It enables the formation of self-induced internal flow through internal passages. The internal flow enters the passage of the hollow blade through the opening near the fan hub and exits through the trailing edge slots at the tip of the hollow blade. The study of the influence of internal flow on the flow field of axial fan and modifications of axial fan aerodynamic characteristics is presented. The characteristics of the axial fan with the internal flow were compared to characteristics of a geometrically equivalent fan without internal flow. The results show integral measurements of performance testing using standardized test rig and the measurements of local characteristics. The measurements of local characteristics were performed with a hot-wire anemometry and a five-hole probe. Reduction in adverse flow conditions near the trailing edge at the tip of the hollow blade, boundary-layer reduction in the hollow blade suction side, and reduction in flow separation were attained. The introduction of the self-induced blowing led to the preservation of external flow direction defined by the blade geometry, which enabled maximal local energy conversion. The integral characteristic reached a higher degree of efficiency. [DOI: 10.1115/1.4000345]*

*Keywords:* axial fan, hollow blade, self-induced blowing, hot-wire anemometry, five-hole probe

## 1 Introduction

Axial fans often show adverse flow conditions at the fan hub and at the tip of the blade. Near the axial fan hub, at the inlet slot location, recirculation flow occurs. Here, the attachment of the blade onto the fan motor is optimized for easy manufacturing, which affects aerodynamic properties. Consequently, a decrease in flow velocity and increase in pressure is present. As a result, radial flow passing from the hub to the tip of the blade has negative effects on the fan efficiency. On the entire blade, the separation of flow on the suction side of the blade occurs. External flow is not able to follow the path of the blades' profile; therefore, it separates from the profile. The thickness of the boundary layer is increased.

A method to reduce these adverse flow conditions by introducing hollow blades is presented. The internal flow enters the hollow blade near the fan hub, and exits it as a free jet at the trailing edge at the tip of the hollow blade (Fig. 1). The internal flow is self-induced as no energy is required and the only driving force is the fan rotation. The internal flow is mainly driven by the centrifugal forces resulting from the fan rotation. The internal flow passage is mainly radial while the flow exits in the axial direction, although the direction of the internal flow is defined by the shape of the hollow blade. Using these modifications, reduction in adverse flow conditions near the trailing edge at the tip of the blade, boundary-layer reduction in the blade suction side, and reduction in flow separation was achieved. The modifications also enable increased local energy conversion and improve fan characteristics. It is to be understood that due to the centrifugal forces acting on the air in the hollow blade, the overpressure is built up on the tip of the hollow blades in the internal passage. This overpressure enables the air to blow from the trailing edge slot into the external

flow. The increased velocity at the location of the trailing edge slot reduces the static pressure in the external flow. This prevents the formation of adverse pressure gradient in the boundary layer.

Internal flow adds energy to the external flow and consequently contributes to the preservation of the flow direction. As a direct result, flow separation from the blade suction side and the thickness of the boundary layer are reduced, which leads to higher fan efficiency. It can be assumed that at the trailing edge of the hollow blade, where mixing of the external and internal flows takes place, stabilization of flow structures is expected.

The concept of reducing the blade wake through trailing edge blowing has been investigated in the literature, where different explanations were proposed. Schlichting [1] developed a method for preventing separation, where additional energy is supplied to the particles of fluid. Suction was applied in the design of aircraft wings [2], where much larger maximum lift values were obtained. Garg [3] presented the use of hollow blades in gas turbines with induced secondary flow circulation, where the main purpose was blade cooling. Murphy et al. [4] experimentally and numerically described the system used in chemical industry for mixing of multiphase fluids. In their research, gas is supplied through the hollow impeller shaft. Gas continues along to every individual blade, where exit slots on the impeller blades in low pressure regions are drilled. Gas mixes with external fluid and influences the flow field in the vicinity. Sutliff et al. [5] and Woodward et al. [6] presented turbofan noise reduction with full-span trailing edge blowing with hollow blades and internal flow in internal radial flow passages.

To understand flow conditions near the blade trailing edge where internal flow mixes with external flow, the boundary-layer theory of Schlichting [1] and free-jet flow theory [1] were used. This theory was compared with the theory of Batchelor [7] and Hinze [8]. It is expected that the external flow better follows the blade shape near the trailing edge at the tip of the hollow blade and that the fan integral characteristic reaches a higher degree of static pressure difference.

Contributed by the Fluids Engineering Division of ASME for publication in the JOURNAL OF FLUIDS ENGINEERING. Manuscript received February 7, 2008; final manuscript received September 28, 2009; published online October 23, 2009. Editor: Joseph Katz.

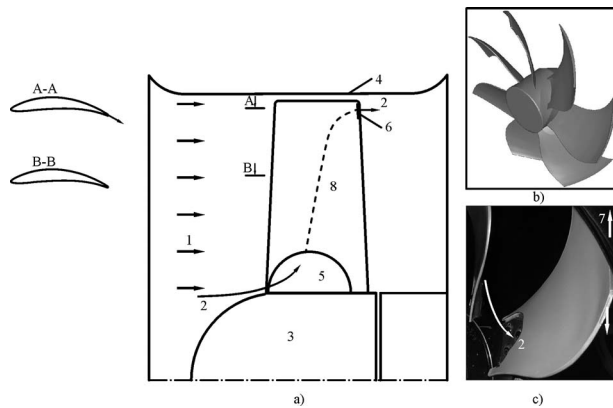


**Fig. 1 Axial fan with self-induced trailing edge blowing: (a) schematic diagram of the axial fan, (b) axial fan, and (c) hollow blade (1. external flow; 2. internal flow; 3. fan rotor; 4. fan casing; 5. inlet opening for internal flow; 6. trailing edge slot at the tip of the hollow blade for internal flow; 7. rotation of the axial fan; 8. hollow blade) [12]**

Changes in the flow field near the fan hub are also expected. They mostly result from the internal flow flowing into the internal radial flow passage; consequently, a reduction in radial flow in the cascade near the fan hub is expected [9–11].

To confirm the above assumptions, two versions were compared differing only in the presence or the absence of blade internal flow. Measurements of the integral characteristic were performed. Both versions were compared by the experimental analysis of local velocity field measurements with a hot-wire anemometry and a five-hole probe. All measurements were performed at equal operating and known ambient conditions.

The results show that the introduction of internal flow improved the fan characteristics and reduced the flow separation on the suction side of the blade.

## 2 Experimental Setup

The tested axial fan had a diameter of 500 mm and was manufactured with seven hollow blades [11,12]. The hub radius of the axial fan was 140 mm and the slot between the hollow blade and influx was 4 mm. The hollow blades were manufactured from serially produced  $\varnothing 500$  mm axial fan blades upon several modi-

fications. The original/conventional axial fan blade was made from the profile NACA 63A series, where only the suction side of the blade was used with 2 mm thickness on the whole surface. Hollow blade had the same profile as the original blade—on the suction side of the hollow blade with 1 mm thickness on the whole surface. For the presented hollow blade, an additional layer of the NACA 63A series suction side with 1 mm thickness on the pressure side of the blade was added. The pressure side of the hollow blade had the same aspect ratio, but smaller curvature, enabling the gap between the suction and pressure sides for internal flow passage. At the tip of the hollow blade, the maximum thickness was 5 mm.

The internal flow enters the internal radial flow passage of the hollow blade through the openings near the fan hub. The inlet slot of the hollow blades has a semicircle opening with a diameter of 40 mm (Fig. 1). The outlet slot on the trailing edge at the tip of the hollow blade, where the internal flow exits the blade internal passages, has a size of  $20 \times 1$  mm (Fig. 1). Therefore, the inlet/outlet surface ratio was approximately 30.

The selection of the fan was based on the results of the flow kinematics analysis of the internal [1] and external flows, as shown in Fig. 2 [13]. Calculations were made for three axial fan operating points at volume flow coefficients of  $\varphi_1=0.24$ ,  $\varphi_2=0.26$ , and  $\varphi_3=0.28$  (Table 1).

In order to estimate the external flow velocity, relative velocity  $w$  was calculated from the velocity vector triangle (Fig. 2(b)). Relative velocity  $w$  is calculated from the axial velocity  $c_{a2}$  and relative velocity angle  $\beta_2$  (Fig. 2(b)). Relative velocity  $w$  is compared with the velocity of the internal flow  $u_j$ .

The estimation of velocity of the internal flow is based on the following three assumptions: (i) internal channel is large enough that no losses inside the hollow blade occur and the pressure at the trailing edge slot is only a result of centrifugal forces; (ii) the pressure at the location of the trailing edge slot is transformed into velocity and the pressure loss coefficient  $\xi$  due to narrowing can be used; and (iii) the velocity at the location of the hot-wire anemometer can be estimated from the velocity in the trailing edge slot using equations from the boundary-layer theory and published experimental results.

For the internal flow, first the determination of pressure and velocity of internal flow in the internal passage was taken into consideration. Pressure in the internal passage is a result of centrifugal forces. The internal passage is large enough that no pressure inside is lost. Through the internal radial flow passage, the

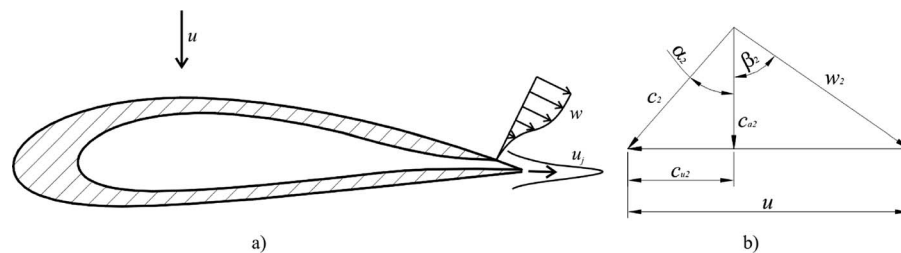


**Fig. 2 (a) Direction and size of the internal  $u_j$  and external  $w$  flow velocities at the blade trailing edge; (b) external flow velocity vector triangle on the blade trailing edge: absolute  $c_2$ , axial  $c_{a2}$ , and tangential  $u$  velocities**

**Table 1 Analytically determined axial fan velocities**

$N$	Volume flow coefficient $\varphi$	Air density $\rho$ (kg/m <sup>3</sup> )	Axial fan motor rotations per minute $n$ (rpm)	External flow velocity $w$ (m/s)	Internal flow pressure $p_j$ (Pa)	Internal flow velocity $u_j$ (m/s)
1	0.24	1.2	1133	25.7	544	29.1
2	0.26	1.2	1129	24.9	541	29.0
3	0.28	1.2	1123	23.7	535	28.8

passage cross section narrows all the way to the tip trailing edge, where the internal flow exits through the trailing edge slot at the tip of the hollow blade. A presumption was made that the internal flow is unimpeded and ideally follows the internal flow passage. In the slot, the pressure is transformed into kinetic energy. Therefore, only loss due to narrowing was considered. Because of narrowing, loss coefficient  $\xi$  is selected analytically [14]. At the exit, where the internal flow from the trailing edge slot at the tip of the hollow blade mixes with the external flow, local velocity is increased and pressure is decreased. Due to the comparison of mathematical analyses of external and internal flows with the measurement results attained from the local measurements with a hot-wire anemometry and a five-hole probe, which were performed 5 mm from the trailing edge of the hollow blade, the theory of Schlichting [1] was used to estimate the velocity at the location where the measurements took place.

When the internal flow exits the trailing edge slot at the tip of the hollow blade, a jet boundary occurs between two streams, which move at different speeds in the same direction. The width of this mixing region increases in a downstream direction. The emerging jet becomes mixed with the surrounding fluid. Particles of fluid from the surroundings are carried away by the jet so that the mass flow increases in the downstream direction. It is permissible to study such problems with the aid of the boundary-layer equations, and with the aid of semi-empirical assumptions, it is possible to apply Prandtl's mixing-length theory [1].

Experimental results on jets were given by the German Aerospace Center in Goettingen [1]. The assumption for shear stress leads to a considerably simpler calculation. The width of the jet is proportional to  $x$  and the center-line velocity  $u_j \sim x^{-1}$ . Thus, according to measurements, the virtual kinematic viscosity  $\varepsilon_0$  is a function of the loss coefficient  $\xi$ , air density  $\rho$ , internal flow pressure  $p_j$ , and width of the jet  $x$ . The virtual kinematic viscosity  $\varepsilon_0$  remains constant throughout the jet. The differential equation for the velocity distribution becomes formally identical with that for the laminar jet, the only difference being the virtual kinematic viscosity of the turbulent flow. The constant kinematic momentum  $K$  was introduced; according to the measurements  $K$  is a function of the loss coefficient  $\xi$ , air density  $\rho$ , internal flow pressure  $p_j$ , and width of the jet  $x$ . Kinematic momentum  $K$ , as a measure of the strength of the jet velocity  $u_j$  of exiting internal flow, was obtained [1] in Eq. (1) as

$$u_j = \text{const} \frac{K}{\varepsilon_0 x} \frac{1}{\left(1 + \frac{1}{4} \eta^2\right)^2} \quad (1)$$

where  $\eta$  in Eq. (2) is defined as [1]

$$\eta = \text{const} \frac{\sqrt{K} y}{\varepsilon_0 x} \quad (2)$$

According to the measurement performed by the German Aerospace Center in Goettingen and Reichardt [1], the empirical solutions of constant values for  $K^{-2}/\varepsilon_0$  were determined.

Table 1 presents analytically determined external flow velocity  $w$  and internal flow velocity  $u_j$  at the exit from the trailing edge slot at the tip of the hollow blade.

Table 1 shows that the internal flow velocity  $u_j$  is greater compared with the external jet flow  $w$  ( $u_j > w$ ), meaning that the internal flow forces the external flow in its direction. At this point, it is important to emphasize that the external flow velocity  $w$  obtained from the velocity vectors presents the velocity in the far-field region from the blade wall (Fig. 2(a)) and proportionally reduces in directions toward the blade wall [1]. Consequently, it can be assumed that the internal flow in the near wall region has an even higher influence toward the external flow; therefore, it is assumed that velocity  $u_j \gg w$ .

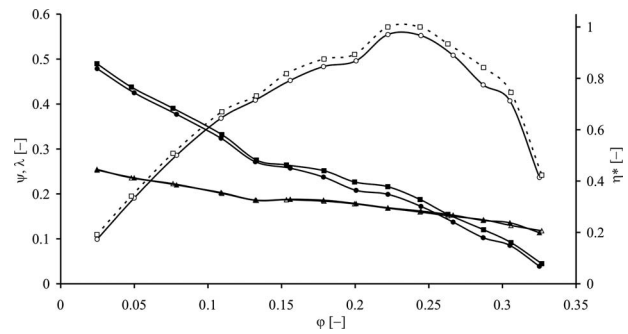


**Fig. 3 Comparison of the integral characteristic of the axial fan at local properties and normalized efficiency for the cases with and without internal flow: (■) total pressure coefficient  $\psi$  for the case with internal flow; (●) total pressure coefficient  $\psi$  for the case without internal flow; (□) normalized efficiency  $\eta^*$  for the case with internal flow; (○) normalized efficiency  $\eta^*$  for the case without internal flow; (▲) power coefficient  $\lambda$  for the case with internal flow; and (△) power coefficient  $\lambda$  for the case without internal flow**

### 3 Experimental Analysis

The experimental part includes measurements of integral characteristics of the fan and measurements of the local properties. The latter were performed with a hot-wire anemometry and a five-hole probe. All measurements were carried out in accordance with standards and under equal ambient conditions. Measurements of both versions with and without internal flows were performed immediately one after another, in a way, which allows achieving minimal measurement uncertainty.

**3.1 Measurements of Integral Characteristics.** Measurements were performed for both versions. To obtain comparable results, the measurements of integral characteristics were performed in accordance with standards [15,16] under equal operating and ambient conditions and at the same fan operating points, with the same measurement equipment, which was calibrated before measurement and were performed immediately one after another. The motor used was the same for both versions and with the following specifications:  $U=400$  V,  $f=50$  Hz,  $P_w=770$  W, and  $I=1.45$  A. The measurements for both versions were performed with the motor's constant speed. Prior to the measurements was the motor being calibrated according to the instructions of the International Organization for Standardization [15]. Measurements on the axial fan with hollow blades were conducted on a specially designed test station for the measurements of integral characteristics at the Hidria Institute Klima. The volume flow was measured on measurement nozzles with a sensor of differential pressure and static pressure in front of the nozzle. The Mensor 6100 sensor was used in both cases. The static pressure difference  $\Delta p_s$  was measured with the same sensor. The Vaisala HMT 330 measuring device for temperature and relative humidity was used to determine the ambient conditions and pertaining air density, while the barometric pressure was measured with the Vaisala PTB 220 measuring device. The connecting electrical power  $P_w$  and the rotating frequency of the fan's rotor were measured in addition to the aerodynamic parameters. Electrical power was measured with the Zimmer LGM450 digital power analyzer and the rotating frequency  $n$  was measured with an HIK IJ measuring device. The main sources of total measurement uncertainty [9,10,17] are uncertainties of the measuring rotating frequency, volume flow, pressure difference, temperature correction, humidity, etc. Overall measuring uncertainty is estimated to be 2.8% from the measured value and is in accordance with the International Organization for Standardization [16].

The integral characteristic of axial fan is presented in Fig. 3. In Fig. 3, measurements of the pressure difference ( $\psi$ =total pressure

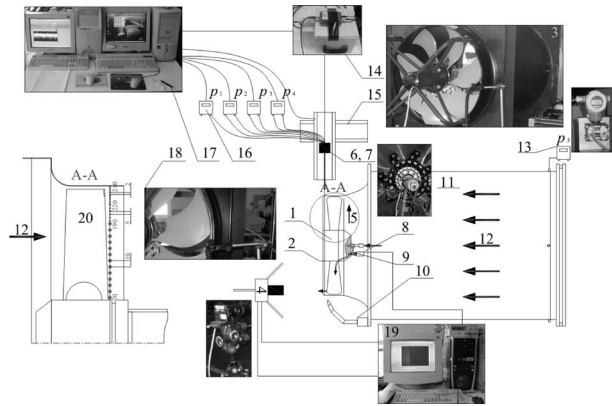


**Fig. 4 Measuring station scheme for measuring local flow properties:** 1. axial flow fan; 2. axial flow fan mesh; 3. wind tunnel with measured axial flow fan; 4. high-speed camera; 5. rotation direction of axial flow fan; 6. five-hole probe; 7. hot-wire anemometer; 8. inductive sensor; 9. rotational speed sensor; 10. illumination, 11. wind tunnel; 12. flow direction indication; 13. differential pressure transmitter; 14. signal conditioning module; 15. positioning table; 16. differential pressure transmitter 1–4; 17. PC for control, acquisition, and data storage 1; 18. axial flow fan with hollow blades and detail; 19. PC for control, acquisition, and data storage 2; and 20. detail (presenting measurement points on a line perpendicular to the axis at a distance of 5 mm behind the trailing edge of the hollow blade)

coefficient), power ( $\lambda$ =power coefficient), and normalized efficiency  $\eta^*$  attained with Eq. (3) are presented. Parameters in the integral characteristic were defined by Eq. (3) as

$$\varphi = \frac{4q_v}{\pi D^2 u}, \quad \psi = \frac{2\Delta p_t}{\rho u^2}, \quad \lambda = \frac{8P_w}{\pi \rho D^2 u^3}, \quad \eta = \frac{\varphi \psi}{\lambda}, \quad \eta^* = \frac{\eta}{\eta_{\max}} \quad (3)$$

where  $\varphi$  is the flow coefficient,  $\psi$  is the total pressure coefficient,  $\Delta p_t$  is the total pressure,  $\lambda$  is the power coefficient,  $P_w$  is the input power from a motor (kW),  $\eta$  is the efficiency,  $\eta^*$  is the normalized efficiency,  $D$  is the diameter,  $\rho$  is the air density, and  $u = \pi D n / 60$  is the velocity.

Figure 3 shows results for the integral characteristics of the axial fan in local properties with and without internal flows. When the internal flow was introduced, an increase in normalized efficiency  $\eta^*$  and pressure coefficient  $\psi$  was observed. A difference in pressure coefficient  $\psi$  (up to 6%) is present through the complete operating range. The power coefficient  $\lambda$  is comparable for both versions.

It can be assumed that the blade wake is reduced, which consequently leads to shifting of the characteristic toward larger values of flow in the complete operating range of the axial fan.

**3.2 Measurements of Local Flow Properties.** Measurements of the local flow properties were performed with a hot-wire anemometer and a five-hole probe. Local measurements were performed in three operating points, at axial fan rotating frequency  $n=1124$  rpm, and at volume flow coefficients of  $\varphi_1=0.24$ ,  $\varphi_2=0.26$ , and  $\varphi_3=0.28$  (Fig. 3).

Figure 4 shows the scheme of the measuring station for measuring the local flow properties. Measurements of the local flow properties were performed at the outlet of the fan. At the each selected operating point of the axial fan, local flow measurements in 29 measuring points on blade radius were performed. Measurement points were selected on a line perpendicular to the axis at a distance of 5 mm behind the trailing edge of the hollow blade (Fig. 4, detail A-A). This allowed measurements across the entire

trailing edge from the rotor hub to the tip of the hollow blade. Measurement results in every measuring point were compared for the case with and without internal flows.

**3.2.1 Velocity Measurements With Hot-Wire Anemometry.** A hot-wire anemometer was used to measure the instantaneous velocity fluctuations, phase average velocities, and turbulence intensity. Measurements were performed in accordance with Bruun [18] and Jørgensen [19].

For measurements with hot-wire anemometry, a Dantec MiniCTA anemometer with wire sensor Dantec 55P11 (diameter of  $\varnothing 5 \mu\text{m}$  and length of 1.25 mm) was used. The hot-wire anemometer working temperature was  $250^\circ\text{C}$ . The positioning of the hot-wire anemometer sensor on the measurement station allowed measurements of the instantaneous meridional velocity. Positioning of the hot-wire anemometer sensor was performed by using a PC controlled precision positioning device. For the acquisition of the hot-wire anemometer signal, a 16-bit data acquisition board from National Instruments was used. The acquisition frequency was 50 kHz. Prior to analog/digital (A/D) conversion, the output of the hot-wire anemometer was filtered with SCXI module by using low pass fourth order Bessel filter with a frequency of 10 kHz. LABVIEW software was used for data acquisition and storage. Calibration of the hot-wire anemometer was performed on the measuring station for the calibration of anemometers. In accordance with King's law [18], the constants  $A=1.9132$ ,  $B=0.8744$ , and  $n=0.4476$  were determined. Temperature correction was applied during calibration and measurements. Temperature was measured using a Pt-100 class A resistance thermometer with four wire connections and Agilent 34970A instrument. Actual velocity was calculated from the hot-wire anemometer output according to King's law equation [18].

Measurements were performed for both versions with the same measurement equipment, which was calibrated before measurement and were performed immediately one after another. The main sources of the total measurement uncertainty [9,10,17] result from the uncertainty of selecting the operating point and the fluctuations, selecting the starting point of positioning, rotational speed of the fan, calibration, positioning of the hot-wire anemometer sensor with a positioning table, linearization, A/D resolution, data acquisition, temperature correction and humidity, and hot-wire anemometer limited frequency response. The adjustments of the main voltage, fan electric motor temperature variations during measurements, and measurement time uncertainty were selected in accordance with recommendations in Ref. [20]. A separating transformer was used to separate the fan power supply from the measurements' power supply. Overall measuring uncertainty of instantaneous velocity was estimated to be 2.8% of the measured value.

**3.2.2 Velocity Vector Measurements With Five-Hole Probe.** Average velocity vectors were measured using a five-hole probe and were performed on a measuring station, as shown in Fig. 4. Operating and measuring points are the same as for the hot-wire anemometer measurements and are described in Sec. 3.2. The response time of the five-hole probe is very slow, while the velocity fluctuations in the fan are very rapid; therefore, the method allows only measurement of time-averaged velocity vectors. All velocity fluctuations from periodic blade movements and pressure pulsations are averaged.

Two presumptions were considered for time averaging, i.e., stationary fluid flow, for each selected operating point, and fluid flow on the fan inlet and outlet is axisymmetrical regarding the axis of fan rotation. In order to satisfy the axisymmetrical conditions, large unimpeded inlet and outlet flow fields had to be assured. The measuring station has a straight inlet flow section of  $1.5D$  and is selected in accordance with the International Organization for Standardization [15].

United Sensor Co. (New Hampshire, USA) type DA-187 probe was used. The measurement procedure using a five-hole probe

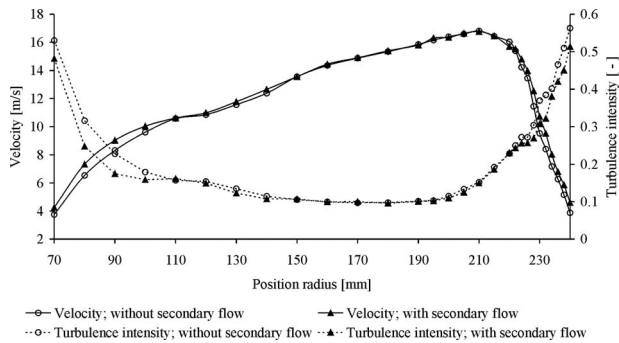


Fig. 5 Average velocity and turbulence intensity in operating point  $\varphi_1=0.24$

requires the manual rotation of the probe around its axis until the yaw angle  $\alpha$  between the axial and tangential velocities of the flow is reached and the pressure difference on the yaw holes is zero. All later measurement steps are performed automatically by reading the measurement transmitters and using calibration curves provided by the manufacturer. From the absolute velocity  $c$  and corresponding angles, axial  $c_a$ , tangential  $u$ , and radial  $v_r$  velocities are calculated.

For differential pressure measurements, a differential pressure transmitter Endress+Hauser Deltabar S PMD75 was used. Absolute pressure was measured with Vaisala PTB 220 while Vaisala HMT 331 transmitter was used for measuring the temperature and relative humidity. Differential pressure transmitters had the current output of 4–20 mA, digitalized with an A/D data acquisition board with 16-bit resolution and sampling frequency of 1 kHz. Sampling data time was 1 min and the measured data from each separate differential pressure transmitter was averaged.

The main sources of the total measurement uncertainty are the uncertainties of the yaw angle measurement [17,21], measurements of ambient conditions, probe positioning, selection of starting position, selection of operating points, velocity and pressure fluctuations, pressure transmitters, data acquisition system, factory calibration curves for five-hole probe, etc. The overall measurement uncertainty was estimated to be 3% for the measurement of velocity and  $\pm 1$  deg for the measurement of flow angles.

## 4 Measurement Results

**4.1 Velocity Measurement Results With Hot-Wire Anemometry.** Figures 5–7 show the average velocities and turbulence intensities, defined as the ratio between the standard deviation and average velocity for the cases with and without internal flows for three different operating points ( $\varphi_1=0.24$ ,  $\varphi_2=0.26$ , and  $\varphi_3=0.28$ ). Measurements were performed using a hot-wire anemometer, as described in Sec. 3.2.1. Here, the velocity is equal

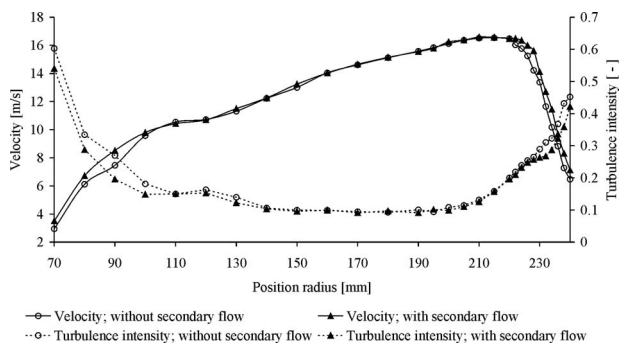


Fig. 6 Average velocity and turbulence intensity in operating point  $\varphi_2=0.26$

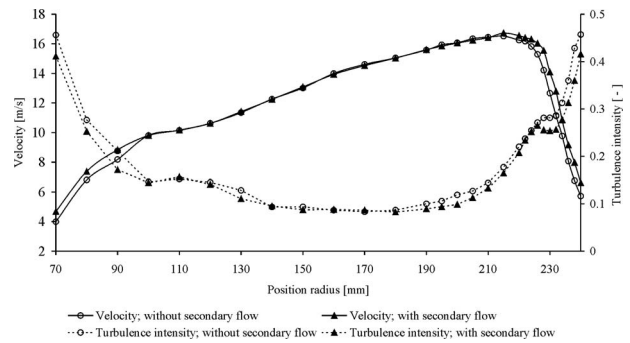


Fig. 7 Average velocity and turbulence intensity in operating point  $\varphi_3=0.28$

to the sum of the axial and radial velocities. Measuring points (20) are positioned from the fan hub, at 70 mm from the fan axis, to the fan tip, at 240 mm from the fan axis. The distances between the measuring points are as follows: from 70 mm to 190 mm from the axis with a step of 10 mm, from 190 mm to 220 mm with a step of 5 mm, and from 220 mm to 240 mm with a step of 2 mm (Fig. 4, detail A-A). Measuring points near the tip of the hollow blade are closer to each other in order to better determine the local flow properties in the region where the internal flow exits the blade internal passage.

In Figs. 5–7, a distinctive difference in average velocity and turbulence intensity between the cases with and without internal flow was noticed.

The difference appears on the blade radius from 210 mm to 240 mm due to internal flow exiting from the trailing edge slot at the tip of the hollow blade and mixing with the external flow. In average, about 7.8% increase in velocity and about 9.1% reduction in turbulence intensity was achieved by the introduction of the internal flow. It is interesting that the introduction of the internal flow also resulted in more beneficial conditions near the hub of the fan (from 70 mm to 100 mm). Velocity is increased in the near hub region in average for about 6.9%. Turbulence intensity is reduced in average for 10%. This reduced the generation of vortices near the fan hub, which is usual for this fan type and used method of attachment of the blades to the hub by riveting.

In the middle of the blade, radius velocity remains practically unchanged while the turbulence intensity reduces in average for 4% in the case with internal flow.

In addition, phase average analysis was performed with MATLAB software. Phase average flow velocity was calculated in a way that velocity was cut into sections, corresponding to one fan blade. Signal was cut in accordance to the fan's rotational speed. Results are presented in Fig. 8. Velocity is presented for the operating point of the axial fan at  $\varphi_2=0.26$  for cases with and without internal flow. Measuring point at a radius of 228 mm was selected. At this radius, the trailing edge slot is located. The velocity dis-

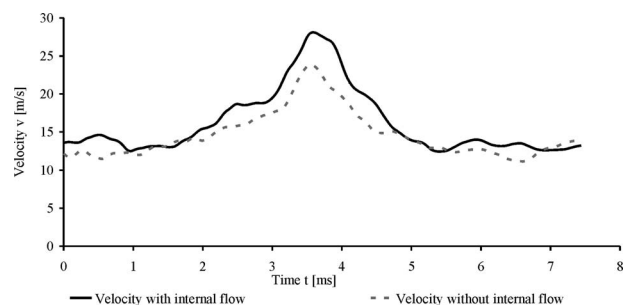


Fig. 8 Phase average of the axial relative velocity field for  $\varphi_2=0.26$  and radius of 228 mm

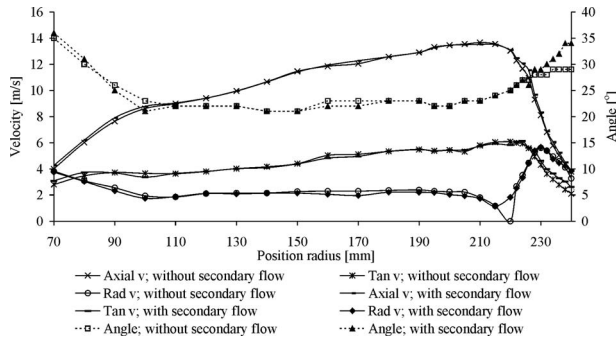


Fig. 9 Axial, tangential, and radial velocities, and yaw angle  $\alpha$  for fan operating point  $\varphi_1=0.24$

tributions for the other two operating points are comparable and are therefore not shown. In the case with internal flow, increased average velocity at the location of the trailing edge of the hollow blade was achieved. The peak of maximum velocity is shifted to the right, which corresponds to higher velocity on the suction side of the hollow blade. Higher velocity on the suction side of the hollow blade shows that the external flow better follows the angle of the hollow blade.

Introduction of the internal flow reduces the turbulence intensity and increases the average velocity in the regions close to the hub and tip of the hollow blade. This occurs because the internal flow adds energy to the external flow and consequently contributes to the preservation of flow direction. As a direct result, flow separation from the blade suction side and thickness of the boundary layer are reduced, which leads to higher fan efficiency.

**4.2 Results of Velocity Measurements With Five-Hole Probe.** Measurements with a five-hole probe were performed with and without internal flows in the same positions and operating points as measurements with hot-wire anemometry. The description of selecting operating and measuring points can be found in Sec. 4.1. Figures 9–11 present the axial  $c_a$ , tangential  $u$ , and radial  $v_r$  velocities and yaw angle  $\alpha$ .

Figures 9–11 show that in the case with internal flow the tangential velocity on the blade trailing edge near the tip of the hollow blade increases in average by 11%. Also, a change in velocity yaw angle  $\alpha$  is substantial as it increases to about 10%. Consequently, the flow direction is changed and that the air flow in the case of the internal flow better follows the contour of the fan blade.

When on a radius from 70–100 mm, a 3% reduction in radial velocity and yaw angle  $\alpha$  is observed. These changes are a result of flow passing into the internal flow passage. As a consequence, external radial flow reduces.

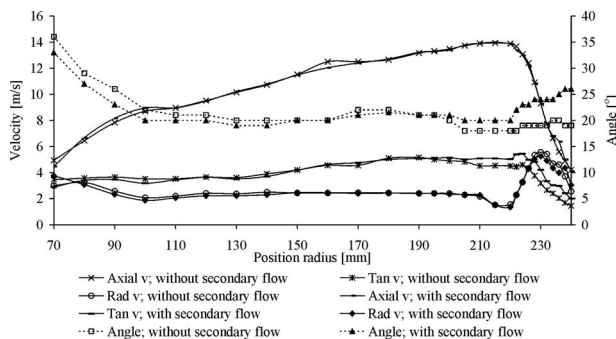


Fig. 10 Axial, tangential, and radial velocities, and yaw angle  $\alpha$  for fan operating point  $\varphi_2=0.26$

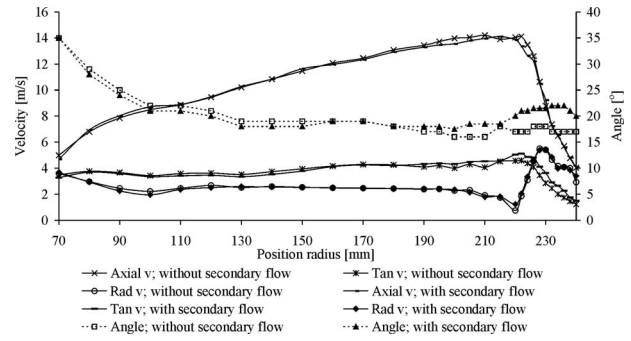


Fig. 11 Axial, tangential, and radial velocities, and yaw angle  $\alpha$  for fan operating point  $\varphi_3=0.28$

In the middle of the blade span (from 100 mm to 200 mm from the axis of the fan), deviations in velocity and yaw angle  $\alpha$  are not distinctive.

Results of measurements with a five-hole probe are in agreement with the results obtained by hot-wire anemometry. Both measurements confirm that the introduction of the internal flow influences the flow through the axial fan with hollow blades.

## 5 Conclusions

This paper presented the introduction of flow through the hollow blades of the axial fan. With the help of different measuring techniques, the effects of the internal flow on the flow field of the hollow blade were determined. As a consequence, increased velocity, reduced turbulence intensity, and more uniform velocity distribution were obtained with the internal flow passing through the hollow blades. It is interesting to know that by introducing the internal flow, more beneficial conditions near the hub of the fan were achieved as well. Velocity increase in the region near the hub is a result of more plausible fluid flow as a part of the external flow, entering the hollow blade internal flow passage. This reduces the generation of vortices near the fan hub, which is usual for this type of fan and for the used method of attaching the blades to the hub by riveting. In the middle of the blade radius, velocity remains practically unchanged while the turbulence intensity reduces in the case with internal flow. Therefore, it is assumed that the external flow field changes and follows the blade contour better; the flow separation near the trailing edge on the suction side at the tip of the hollow blade minimizes. The beneficial influence also reflects in the integral characteristic, where increase in static pressure difference was achieved.

## Nomenclature

- $A$  = King's law constants
- $B$  = King's law constants
- $c$  = velocity (m/s)
- $D$  = diameter (mm)
- $f$  = frequency (Hz)
- $I$  = current (A)
- $n$  = fan rotation ( $\text{min}^{-1}$ )
- $n$  = King's law constants
- $p$  = pressure (Pa)
- $P$  = power (kW)
- $u$  = velocity (m/s)
- $U$  = voltage (V)
- $w$  = relative velocity (m/s)
- $q$  = flow ( $\text{m}^3/\text{h}$ )
- $v$  = velocity (m/s)
- $\Delta$  = difference
- $\alpha$  = jaw angle (deg)
- $\beta$  = pitch angle (deg)
- $\eta$  = efficiency

$\varphi$  = flow coefficient  
 $\rho$  = air density ( $\text{kg}/\text{m}^3$ )  
 $\xi$  = loss coefficient  
 $\lambda$  = power coefficient  
 $\psi$  = total pressure coefficient

### Subscripts

$a$  = axial  
 $j$  = internal jet flow pressure  
 $r$  = radial  
 $s$  = static  
 $t$  = total  
 $u$  = axial component of tangential velocity  
 $v$  = volume

### References

- [1] Schlichting, H., 1979, *Boundary-Layer Theory*, Springer, Berlin.
- [2] Rhee, S. H., Kim, S. E., Ahn, H., Oh, J., and Kim, H., 2003, "Analysis of a Jet-Controlled High-Lift Hydrofoil With a Flap," *Ocean Eng.*, **30**, pp. 2117–2136.
- [3] Garg, V. K., 2002, "Heat Transfer Research on Gas Turbine Airfoils at NASA GRC," *Int. J. Heat Fluid Flow*, **23**, pp. 109–136.
- [4] Murthy, B. N., Deshmukh, N. A., Patwardhan, A. W., and Joshi, J. B., 2007, "Hollow Self-Inducing Impellers: Flow Visualization and CFD Simulation," *Chem. Eng. Sci.*, **62**, pp. 3839–3848.
- [5] Sutliff, D. L., Tweedt, D. L., Fite, B. E., and Envia, E., 2002, *Low-Speed Fan Noise Reduction With Trailing Edge Blowing*, Glenn Research Center, Cleveland, OH.
- [6] Woodward, R. P., Fite, E. B., and Podboy, G. G., 2007, *Noise Benefits of Rotor Trailing Edge Blowing for a Model Turbofan*, Glenn Research Center, Cleveland, OH.
- [7] Batchelor, G. K., 2000, *An Introduction to Fluid Dynamics*, Cambridge University Press, Cambridge.
- [8] Hinze, J. O., 1959, *Turbulence: An Introduction to Its Mechanism and Theory*, McGraw-Hill, New York.
- [9] Eberlinc, M., Širok, B., and Hočevvar, M., 2009, "Experimental Investigation of the Interaction of Two Flows on the Axial Fan Hollow Blades by Flow Visualization and Hot-Wire Anemometry," *Exp. Therm. Fluid Sci.*, **33**(5), pp. 929–937.
- [10] Eberlinc, M., Širok, B., Hočevvar, M., and Dular, M., 2009, "Numerical and Experimental Investigation of Axial Fan With Trailing Edge Self-Induced Blowing," *Forsch. Ingenieurwes.*, **73**(3), pp. 129–138.
- [11] Eberlinc, M., Širok, B., and Hočevvar, M., 2009, "Patented Hollow Blades of the Axial Fan With Trailing Edge Self-Induced Blowing," *Bentham Science Publishers Recent Patents on Mechanical Engineering*, **2**(1), pp. 1–7.
- [12] Eberlinc, M., Širok, B., Hočevvar, M., and Dular, M., 2009, "Axial Turbine Machine Hollow Blade With Internal and External Flow Field," The Slovenian Intellectual Property Office, Patent No. 22635.
- [13] Wallis, R. A., 1983, *Axial Fans and Ducts*, Wiley, New York.
- [14] Idelčik, I. E., 1991, *Fluid Dynamics of Industrial Equipment: Flow Distribution Design Methods*, Hemisphere, New York.
- [15] International Organization for Standardization, 2007, ISO 5801: 2007: Industrial Fans.
- [16] International Organization for Standardization, 2003, ISO 5167: 2003: Measurement of Fluid Flow.
- [17] Coleman, H. W., and Steele, W. G., 1989, *Experimentation and Uncertainty Analysis for Engineers*, Wiley, New York.
- [18] Bruun, H. H., 1995, *Hot-Wire Anemometry Principles and Signal Analysis*, Oxford University Press, New York.
- [19] Jørgensen, F. E., 2005, *How to Measure Turbulence With Hot-wire Anemometers*, Dantec Dynamics, Skovlunde.
- [20] Verein Deutscher Ingenieure/Verband Deutscher Elektro-Techniker, 1993, "Netzmessungen in Strömungsquerschnitten," Paper No. VDI/VDE 2640.
- [21] Gonzalez, J. C., and Arrington, E. A., 1999, *Five-Hole Flow Angle Probe Calibration for the NASA Glenn Icing Research Tunnel*, Dynacs Engineering Company, Inc., Brook Park, OH.